Journal of Advances in Modeling Earth Systems

RESEARCH ARTICLE
10.1002/2017MS001223

# Modeling Global Ocean Biogeochemistry With Physical Data Assimilation: A Pragmatic Solution to the Equatorial Instability

**Jong-Yeon Park[1,2], Charles A. Stock[2], Xiaosong Yang[2], John P. Dunne[2], Anthony Rosati[2], Jasmin John[2], and Shaoqing Zhang[3]**

[1]Atmospheric and Oceanic Sciences Program, Princeton University, Princeton, NJ, USA, [2]National Oceanic and Atmospheric Administration/Geophysical Fluid Dynamics Laboratory, Princeton, NJ, USA, [3]Physical Oceanography Laboratory/CIMST, Ocean University of China and Qingdao National Laboratory for Marine Science and Technology, Qingdao, China

**Key Points:**
- Physical data assimilation causes marked degradation of simulated equatorial marine biogeochemistry due to spurious vertical velocities
- This issue can be addressed by weighting model over data constraints in a narrow band around the equator
- Off-equatorial data constraints still improve physical and biogeochemical simulations relative to nonassimilative control simulation despite down weighting of equatorial data

**Supporting Information:**
- Supporting Information S1

**Correspondence to:**
J.-Y. Park,
jongyeon@princeton.edu

**Citation:**
Park, J.-Y., Stock, C. A., Yang, X., Dunne, J. P., Rosati, A., John, J., et al. (2018). Modeling global ocean biogeochemistry with physical data assimilation: A pragmatic solution to the equatorial instability. *Journal of Advances in Modeling Earth Systems*, *10*, 891–906. https://doi.org/10.1002/2017MS001223

Received 30 OCT 2017
Accepted 7 MAR 2018
Accepted article online 12 MAR 2018
Published online 30 MAR 2018



**Abstract** Reliable estimates of historical and current biogeochemistry are essential for understanding past ecosystem variability and predicting future changes. Efforts to translate improved physical ocean state estimates into improved biogeochemical estimates, however, are hindered by high biogeochemical sensitivity to transient momentum imbalances that arise during physical data assimilation. Most notably, the breakdown of geostrophic constraints on data assimilation in equatorial regions can lead to spurious upwelling, resulting in excessive equatorial productivity and biogeochemical fluxes. This hampers efforts to understand and predict the biogeochemical consequences of El Niño and La Niña. We develop a strategy to robustly integrate an ocean biogeochemical model with an ensemble coupled-climate data assimilation system used for seasonal to decadal global climate prediction. Addressing spurious vertical velocities requires two steps. First, we find that tightening constraints on atmospheric data assimilation maintains a better equatorial wind stress and pressure gradient balance. This reduces spurious vertical velocities, but those remaining still produce substantial biogeochemical biases. The remainder is addressed by imposing stricter fidelity to model dynamics over data constraints near the equator. We determine an optimal choice of model-data weights that removed spurious biogeochemical signals while benefitting from off-equatorial constraints that still substantially improve equatorial physical ocean simulations. Compared to the unconstrained control run, the optimally constrained model reduces equatorial biogeochemical biases and markedly improves the equatorial subsurface nitrate concentrations and hypoxic area. The pragmatic approach described herein offers a means of advancing earth system prediction in parallel with continued data assimilation advances aimed at fully considering equatorial data constraints.

## 1. Introduction

Current state-of-the-art global ocean models can successfully simulate many aspects of large-scale ocean circulation and its variability. Biases due to imperfect representation of ocean processes and forcing, however, persist across regional and ocean-basin scales (Danabasoglu et al., 2014; Griffies et al., 2014; Large & Yeager, 2009). In addition, ocean prediction efforts require initializations that, to the extent possible, contain dynamics (i.e., waves and instabilities) that are in phase with those observed. Data assimilation aims to improve estimates of ocean conditions by combining diverse observations with the dynamical equations embedded in ocean models. In recent decades, ocean data assimilation systems have advanced considerably from a largely experimental endeavor to a key element of operational ocean retrospective state estimates, nowcasts, and seasonal to multiannual forecasts (Balmaseda et al., 2013; Behringer et al., 1998; Carton & Giese, 2008; Chang et al., 2013; Hoteit et al., 2010; Kohl & Stammer, 2008; Saha et al., 2014; Storto et al., 2016; Yang et al., 2013; Zhang et al., 2007).

Improved ocean data assimilation and prediction has spurred expanding applications beyond inference of physical properties, such as phytoplankton biomass monitoring, ocean carbon cycle monitoring/assessment, and marine resource management (Brasseur et al., 2009; Tommasi et al., 2017a, 2017b). Physical properties (e.g., temperature and salinity anomalies) often provide useful proxies for marine resource responses for limited periods, but such relationships eventually break down (Myers, 1998). More holistic estimates and predictions of ecosystem state are needed for robust prediction. Such efforts are further motivated by

potentially abrupt changes in ecosystem states (Mollmann et al., 2015) and the potential for ecosystem processes to amplify subtle changes in physical or lower trophic level perturbations (Chust et al., 2014; Kearney et al., 2013; Stock et al., 2014a, 2017).

While there is a clear need for biogeochemical assimilation and prediction, the field is less mature than its physical counterpart. This reflects an array of added challenges including uncertainties originated from the representation of physical and biogeochemical processes in earth system models, relatively sparse global-scale observations of subsurface biogeochemical variables, and the large number of biogeochemical tracers that increase the complexity of relationships between observed variables and those that need to be inferred. In addition, the large positive skewness of biological variables often violates the Gaussian distribution assumption used in some data assimilation approaches (Edwards et al., 2015; Hawkins & Sutton, 2009; Song et al., 2016).

Another serious impediment to progress toward fully coupled physical-biogeochemical data assimilation is the extremely high sensitivity of ocean biogeochemistry to spurious vertical velocities that can arise due to dynamical imbalances induced during data assimilation (Anderson et al., 2000; Raghukumar et al., 2015). Across most of the global ocean, the exchange of nutrients between the nutrient-rich ocean interior and well-lit but nutrient-poor surface ocean is tightly regulated by a sharp pycnocline and associated sharp nutricline. Even small spurious vertical transports across this surface can have disastrous impacts on biogeochemical states. This issue has proven to be most acute along the equator, where the dominant geostrophic balance shaping large-scale ocean circulation breaks down. Without this dynamical constraint, perturbations to the ocean density field introduce a shock that can induce waves and instabilities similar to those generated by westerly wind bursts (Balmaseda et al., 2007; Bell et al., 2004; Burgers et al., 2002; Vidard et al., 2007; Waters et al., 2017; While et al., 2010).

Previous studies have proposed several possible approaches to improve the performance of assimilative models at the equator. For example, Burgers et al. (2002) hypothesized that the poor performance of data assimilation for velocity fields is due to the lack of balance in the data assimilation updates near the equator. They used an extended "geostrophic" relationship and applied east-west velocity increments together with height increments. Bell et al. (2004) suggested a pressure correction scheme to update slowly evolving bias fields, which aims to dampen spurious circulations during assimilation. They calculated a bias-corrected pressure field from temperature and salinity biases, and then applied it in the horizontal momentum equations. Waters et al. (2017) proposed a new approach, named as incremental pressure correction scheme, to balance equatorial increments and to reduce initialization shock, which is based on the pressure correction scheme suggested by Bell et al. (2004), but applied over shorter time scales. Although these studies show positive results, the spurious velocity problem has not been satisfactorily resolved enough to prevent the bias in sensitive biogeochemistry variables.

The range of challenges described in the preceding paragraphs has led many biogeochemical assimilation efforts to adopt idealized model frameworks or to focus on regional scales where ocean biogeochemical observing systems are well established (Ciavatta et al., 2014; Fontana et al., 2009; Hemmings et al., 2008; Ishizaka, 1990; Natvik & Evensen, 2003; Pelc et al., 2012; Shulman et al., 2013). A few pioneering studies, however, have tested global-scale biogeochemical assimilation (Ford & Barciela, 2017; Ford et al., 2012; Gregg, 2008; Gregg et al., 2017; Valsala & Maksyutov, 2010; While et al., 2012). These studies assimilate a single biogeochemical variable—either satellite-retrieved chlorophyll data or observed $pCO_2$ data—into a global ocean model and show a general improvement of their related biogeochemical prognostic variables compared with unconstrained model simulations. The effects of spurious vertical motions on biogeochemical variables are limited by biogeochemical assimilation in data-rich regions, but such corrections hinder interpretation of data assimilative hindcasts, become more difficult with increasing biogeochemical complexity, and do not limit impacts in data-poor regions.

The purpose of this study is to investigate approaches for integrating global biogeochemistry and data assimilative ocean physics that address the issue of spurious vertical velocity while still gaining benefits from improved ocean state estimation. We start from a baseline solution integrating a 33 tracer ocean biogeochemical model (Stock et al., 2014b) with an established global ocean data assimilation system that is based on an ensemble Kalman Filter (EnKF) approach applied to the ocean and atmosphere (Zhang et al., 2007). Predictably, the equatorial biogeochemistry of this baseline integration is severely degraded relative

to nondata assimilative models due to spurious vertical velocities along the equator, as discussed above. We then consider two means of overcoming this issue. First, noting that the primary dynamical balance at the equator is between the wind and the zonal pressure gradient, we assess the impact of strengthening data constraints on the atmospheric state estimation. We will show that this reduces, but does not fully address, the issue of spurious vertical velocity.

For our second series of experiments, we consider the effect of modulating the relative weighting of the model and the observations in the data assimilation process. Data assimilation rests on the hypothesis that the true ocean state lies between the model and observations, with weightings chosen according to the relative confidence on each. Given the high sensitivity of ocean biogeochemistry to spurious vertical motions arising from dynamical imbalances introduced by data assimilation, an additional pragmatic approach that can be considered is to impose stricter fidelity to the dynamical model solution. Our experiments thus answer two critical questions: (1) how strongly must one weight the dynamical model solution relative to the observations in the vicinity of the equator to eliminate spurious vertical velocities? and (2) does data assimilation still offer meaningful physical and biogeochemical improvements relative to the nonassimilative case at the threshold determined by question 1? We find that it is indeed still possible to improve physical and biogeochemical state estimates while down-weighting observations at the equator. We then discuss the implications of this result for biogeochemical state estimation, highlighting the potential benefits of improved physical data assimilation for biogeochemical prediction.

## 2. Methods

### 2.1. Model

This study uses the Geophysical Fluid Dynamics Laboratory (GFDL) ensemble coupled data assimilation system (ECDA). The ECDA employs GFDL's fully coupled atmosphere-land-sea ice-ocean model (CM2.1), and an ensemble Kalman filter assimilation scheme is applied to the coupled model (Delworth et al., 2006; Zhang et al., 2007). The horizontal resolution of the atmosphere and land models is 2.5° longitude × 2° latitude on a regular grid, while the ocean and sea ice models have the resolution of 1° with telescoping to 1/3° meridional spacing near the equator. In the ECDA, both atmosphere and ocean states are constrained by observations, which ensures a better-balanced state between atmosphere and ocean variables than if only one component of the climate system is constrained. All simulations using the ECDA are run with a 12 member ensemble that is used to estimate the probability distribution function of climate states.

The ocean in the ECDA is constrained by in situ ocean temperature and salinity observations that include oceanic profiles (XBT, CTD, OSD, MBT, and MRB) from World Ocean Database (WOD), Argo profiles since 2000, and global temperature-salinity profile program (GTSPP) data sets since 2009. Daily SST obtained from NOAA optimum interpolation SST v2 high-resolution data set is also used in the ECDA (Reynolds et al., 2007). The horizontal correlation scale is 10° for both longitude and latitude that is multiplied by a cosine function of latitude up to 80°N (S). This setting allows the correlation scale to be consistent with the characteristics of the Rossby deformation radius for a global analysis scheme. Given that salinity observations are more sparse than temperature data, ECDA uses pseudosalinity obtained from the predetermined temperature-salinity relationship for the period 1993–2002 (Chang et al., 2011).

The atmosphere in the ECDA is constrained by the National Centers for Environmental Prediction, Department of Energy (NCEP-DOE) Reanalysis 2 (Kanamitsu et al., 2002). The 6 h mean atmospheric winds and temperature are assimilated in the ECDA. The correlation scale employed in the atmospheric data assimilation is 500 km for both winds and temperature, which is the location-independent horizontal scale. More details on the ECDA can be found in Zhang et al. (2007) and Chang et al. (2013).

The Carbon, Ocean Biogeochemistry and Lower Trophics (COBALT) (Stock et al., 2014b) ecological model is integrated with the ECDA to drive ocean biogeochemistry in these physically constrained ocean simulations. COBALT considers 33 tracers to resolve global-scale carbon, nitrogen, phosphorus, iron, and silica cycles with three phytoplankton and three zooplankton groups, which can be coupled with fisheries food web models (Watson et al., 2015). Chlorophyll simulated from COBALT is used to estimate shortwave attenuation coefficients that determine the vertical shortwave heating in the ocean. Global ocean simulations with COBALT have been shown to capture the observed large-scale biogeochemical patterns across ocean biomes (Stock et al., 2014b; Tagliabue et al., 2016).

### 2.2. Experiments

Our baseline data assimilation experiment, referred to as DA-BGC, is the default assimilation run used for physical climate applications of ECDA coupled with the biogeochemical model. This run is notable for having relatively permissive atmospheric constraints (Table 1) that allow the atmosphere to respond more freely to changes in ocean state, but also make the assimilation more vulnerable to atmospheric drift. The data assimilation experiment was integrated for the period 1990–2015 and we analyzed the last 25 years of data excluding the first 1 year spin-up period.

The second data assimilation run, referred to as DA-BGC_Atm, uses the same model configuration as DA-BGC but lowers the error estimates on the atmospheric data constraints. As described in section 1, the intent of this run is to test whether more stringent data constraints on the atmospheric state can reduce dynamical inconsistencies in the equatorial wind-pressure gradient balance generating spurious vertical velocities. This stringent atmospheric data constraint is made by dividing observational standard errors of atmospheric winds and temperature by 10.

Our third set of experiments build off the DA-BGC_Atm configuration. We modified the strength of ocean data constraint in the equatorial region relative to the model constraint by inflating the observational data uncertainty by a factor *f* that is ramped up linearly from the 10° latitude to the equator. We varied the inflation of the data uncertainty from the default setting of 0.5°C to an extreme value of $10^6$°C, with an equal inflation of temperature and salinity fields. Larger data inflation values essentially replace strong adjustments to individual data points at the equator with weaker or negligible adjustments to correct for lower frequency biases without overly strong dynamical perturbations at any given point. A similar approach without data assimilation in the equatorial region has been qualitatively explored in an unpublished work (Ford & Barciela, 2015). The original model-data weights (i.e., 0.5°C for temperature and 0.1 g $kg^{-1}$ for salinity) were maintained throughout the rest of the global ocean. While we modulated the observational variance to shift the weighting of the observations relative to dynamical fidelity with the model, we note that an equivalent result could be obtained by reducing the model uncertainty. Either approach is consistent with intent of the experiment: to impose stricter fidelity to the dynamical model at the equator in recognition of the high sensitivity of biogeochemical results to spurious vertical velocities. We completed this set of experiments by examining the sensitivity of our solution to the latitudinal extent of the elevated observational error, testing lower (2° band north and south of the equator) and upper (20° band). Due to computational limitations, sensitivity experiments testing relative weightings of model versus data were shorter duration (2001–2005).

For each setting of data assimilation experiments, we assessed the model's fidelity with both physical and biogeochemical fields from the observations. The observed temperature field used for the assessment is obtained from the EN4 data sets (Good et al., 2013). The observed nitrate and oxygen are obtained from World Ocean Database (WOD) and the chlorophyll concentration is from the satellite-based ocean color sensors, Sea-viewing Wide Field-of-view Sensor (SeaWiFS) and Moderate Resolution Imaging Spectroradiometer (MODIS) (Esaias et al., 1998; McClain et al., 1998). Unlike the nitrate and oxygen, the satellite chlorophyll data provide only near-surface information.

**Table 1**
*Summary of Experiments*

| Experiment name | Observation errors | Description |
|---|---|---|
| DA-BGC | Atmos: 1 m $s^{-1}$ (Wind), 1 K (Temp)<br>Ocean: 0.5 K (Temp), 0.1 g $kg^{-1}$ (Salinity) | Baseline assimilation run |
| DA-BGC_Atm | Atmos: 0.1 m $s^{-1}$ (Wind), 0.1 K (Temp)<br>Ocean: 0.5 K (Temp), 0.1 g $kg^{-1}$ (Salinity) | Strong atmosphere data constraint<br>Strong atmosphere data constraint |
| DA-BGC_opt | Atmos: 0.1 m $s^{-1}$ (Wind), 0.1 K (Temp)<br>Ocean_eq[a]: 100 K (Temp), 20 g $kg^{-1}$ (Salinity) | Strong atmosphere data constraint<br>+<br>Weak equatorial ocean data constraint |
| CTRL | Atmos: 0.1 m $s^{-1}$ (Wind), 0.1 K (Temp) | Control run<br>No ocean data assimilation |

[a]Error inflation values ramped up linearly to specified values from the 10° latitude to the equator. Error values elsewhere are set to DA-BGC_Atm values.

Our analysis focuses on the subsurface biogeochemistry in the top few hundred meters due to the relatively short period of integration in the assimilation runs. Based on the assessment of the model performance on mean and variability of physical/biogeochemical fields, the optimal combination of atmosphere and ocean data constraints is chosen, named as DA-BGC_opt. This optimal assimilation run is run for the full period 1990–2015 and used for further analysis of simulated marine biogeochemistry.

To assess whether the optimal data assimilation still offers improvements relative to nonassimilative retrospective experiments, a control simulation, referred to as CTRL, is also conducted. In this run, the ocean data assimilation process is switched off, thus the model is guided only by assimilated atmospheric fields using the strong atmospheric constraint settings (Table 1). The 26 year long run with atmosphere-only assimilation was looped three times and the data from the last cycle is used. This setup can be comparable to the Common Ocean-ice Reference Experiment (CORE) protocol (Griffies et al., 2009), which is a standard tool for analyzing past global ocean and biogeochemical variability (Griffies et al., 2014; Henson et al., 2010; Lee et al., 2014).

All data assimilation experiments were started from the same initial condition. For the initialization of physical fields, a restart on 1 January 1990 produced by GFDL's 1960–2015 reanalysis experiment of the ECDA is used (Chang et al., 2013). For the initialization of biogeochemical field, the Global Data Analysis Project (GLODAP) product is used for carbon system (DIC, Alk), the World Ocean Atlas (WOA) data for macronutrients ($NO_3$, $PO_4$, $SiO_4$) and $O_2$ (Garcia et al., 2010a, 2010b; Key et al., 2004). The initialization of other biogeochemical variables was drawn from the control simulation described in Stock et al. (2014b). The nonassimilative run, CTRL, is initialized from the same biogeochemical initial condition as data assimilation runs.

## 3. Degradation of Marine Biogeochemistry With Data Assimilation

The climatological annual means of modeled biogeochemical variables are compared with observations in Figure 1. The control simulation without ocean data assimilation, CTRL, captures large-scale spatial patterns in surface nitrate, subsurface oxygen, and surface chlorophyll. High nitrate and chlorophyll concentrations in the tropics/high latitudes and the subsurface oxygen minimum zone averaged in 200–600 m depth are fairly well represented. There are, however, substantial model discrepancies such as the overestimation of subsurface oxygen in the Southern Ocean, overestimation of the intensity of hypoxia (defined here as $<2$ mL/L) in the eastern equatorial Pacific and underestimation of its westward extension, and overestimation of tropical chlorophyll concentration. Overall results from CTRL show similar performance to those

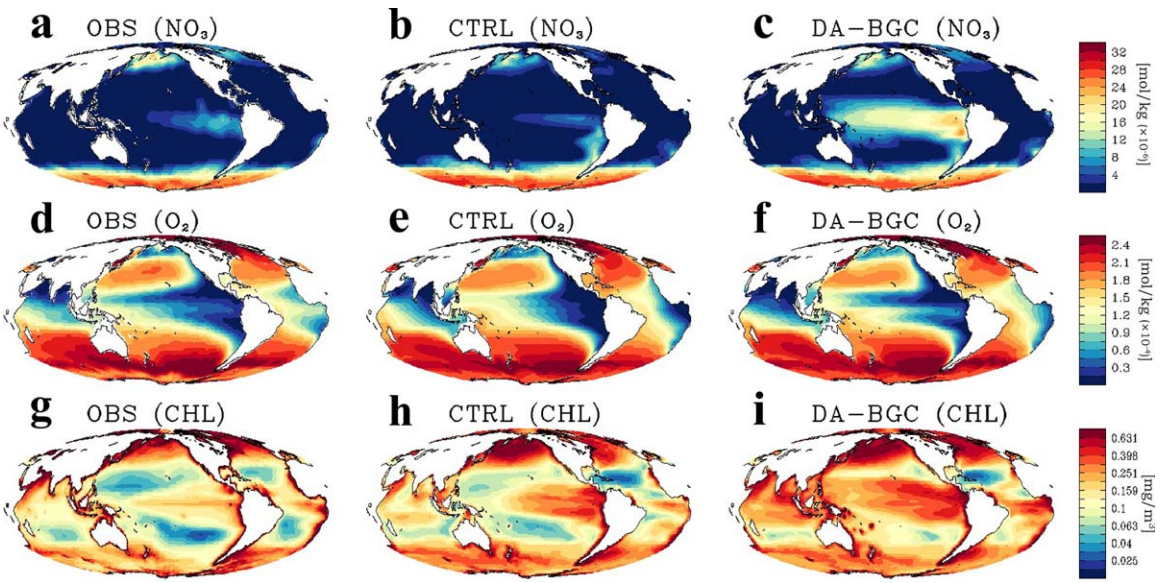


**Figure 1.** Annual mean surface nitrate from the (a) observations, (b) control run (CTRL), and (c) data assimilation (DA-BGC) runs integrated with an ocean biogeochemical model. Plots (d–f) and (g–i) are similar to (a–c) except for subsurface oxygen averaged in 200–600 m depth and surface chlorophyll, respectively.

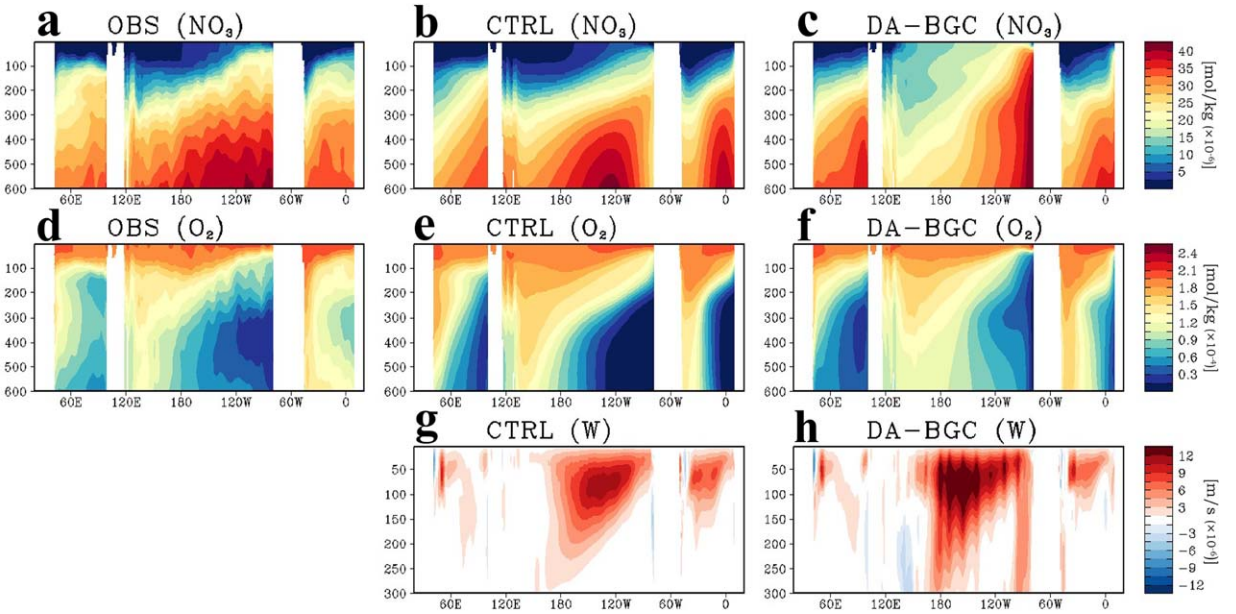


**Figure 2.** Equatorial section of annual mean nitrate from the (a) observations, (b) CTRL, and (c) DA-BGC. Plots (d–f) are similar to (a–c) except for oxygen. Plots (g–h) are similar to (b–c) except for vertical velocity.

from CORE-forced ocean model run (supporting information Figure S1), supporting the use of control run as a natural benchmark to gauge improvements compared to data assimilation runs.

In the baseline assimilation run, DA-BGC, simulated biogeochemical variables generally show marked discrepancies with observations, particularly in the tropics. The simulated tropical nitrate and chlorophyll concentrations in DA-BGC are particularly severe, with substantially higher than those in CTRL and observations (cf. Figures 1a–1c, and 1g–1i). Data assimilation improves the spatial patterns of subsurface oxygen in the tropical Pacific (Figure 1f), but an over-estimate of eastern Pacific oxygen has replaced the under-estimate present in CTRL.

The degradation of biogeochemical variables in the DA-BGC run at the equator is also apparent in the vertical structure of equatorial biogeochemistry (Figure 2). In contrast to the CTRL run, which captures the vertical structures of equatorial nitrate and oxygen averaged between 2°S and 2°N, the DA-BGC run severely over-estimates nitrate above 200 m while under-estimating nitrate below 200 m, implying enhanced nutrient flux into the upper layer from the deeper oceans in DA-BGC. Iron, a critical limiting nutrient in the equatorial Pacific, is also provided by subsurface supply, resulting in excessive surface iron (not shown) and the high surface chlorophyll concentration in DA-BGC (Figure 1i). In addition to degraded nutrient fields, the simulated subsurface oxygen in the equatorial Pacific exhibits an upward shift of hypoxic center and substantially higher oxygen compared to the observation. Despite the overall degradation of biogeochemistry simulation in DA-BGC, some regional improvements are observed in the Atlantic and Indian Ocean basins.

The degradation of simulated marine biogeochemistry after integration with physical data assimilation is associated with increased magnitude and zonal structure in vertical velocities at the equator. The assimilation run features stronger upwelling compared to CTRL (cf. Figures 2h and 2g). This enhanced vertical velocity is consistent with the spurious upwelling issue with data assimilation documented in previous studies (e.g., Bell et al. 2004, Burgers et al. 2002; Waters et al. 2017). Assimilation of observed data into an ocean model near the equator causes a dynamically unbalanced state, which leads to a relatively poor simulation of zonal currents and spurious vertical velocity. The large vertical velocity causes increased upwelling of nutrients, leading to excessive chlorophyll concentrations and increased subsurface oxygen through increased ventilation. A nitrate budget analysis confirms that the excessive nitrate in the equatorial region is dominated by the vertical advection of nitrate (supporting information Figure S2). As shown in Figure 1, the momentum imbalance problem after assimilation is not apparent away from the equator. This is because that geostrophic adjustment plays an important role in balancing ocean and atmosphere updates

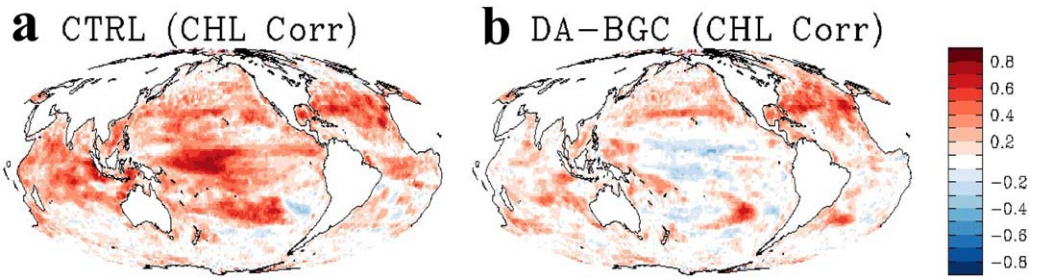


**Figure 3.** Temporal correlation maps of simulated chlorophyll from (a) CTRL and (b) DA-BGC with satellite-retrieved chlorophyll concentrations. The correlation coefficients are calculated after removing monthly climatology during the analyzed period September 1997 to December 2015. The satellite chlorophyll data are bilinearly interpolated onto the regular 1.0° × 1.0° model grid before calculating correlation coefficient.

in the off-equatorial regions, preventing severe degradations of simulated velocity and biogeochemical fields.

In addition to the comparison of mean state, variability of simulated marine biogeochemistry is also compared with observations (Figure 3). The satellite-derived chlorophyll concentration provides a global-scale multiyear record, thus this data set is used to examine the performance of the model in reproducing historical chlorophyll variability. It is found that the CTRL run can simulate the observed chlorophyll variability, albeit modestly in many regions. The correlation coefficient is particularly high over the equatorial central Pacific, where wind-driven ocean dynamical processes play a dominant role in determining surface temperature and chlorophyll. In contrast, the DA-BGC run fails to reproduce the historical variability of tropical chlorophyll concentration, exhibiting negative correlation coefficients in most parts of the equatorial Pacific. This degradation is consistent with a failure to simulate interannual variability of vertical processes associated with equatorial primary productivity.

## 4. Methods for Reducing Equatorial Marine Biogeochemistry Biases

### 4.1. Impact of Wind Bias on Marine Biogeochemistry

The baseline DA-BGC experiment, which includes relatively loose atmospheric constraints (see section 2 and Table 1), results in stronger trade winds in the tropical Pacific compared to the NCEP2 reanalysis (Figure 4). This stronger easterly intensifies poleward mass transport and equatorial upwelling, consistent with the result in Figure 2h. Such biases would also enhance dynamical inconsistencies between assimilated data (reflecting weaker easterlies) and the dynamical model solution, potentially exacerbating spurious vertical velocities.

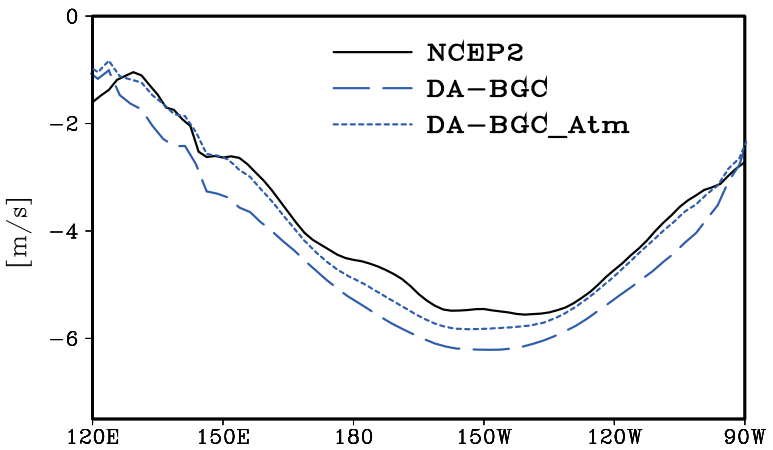


**Figure 4.** Equatorial Pacific trade winds (10 m zonal mean wind averaged between 15°S and 15°N) from NCEP2 reanalysis, DA-BGC, and DA-BGC_Atm.

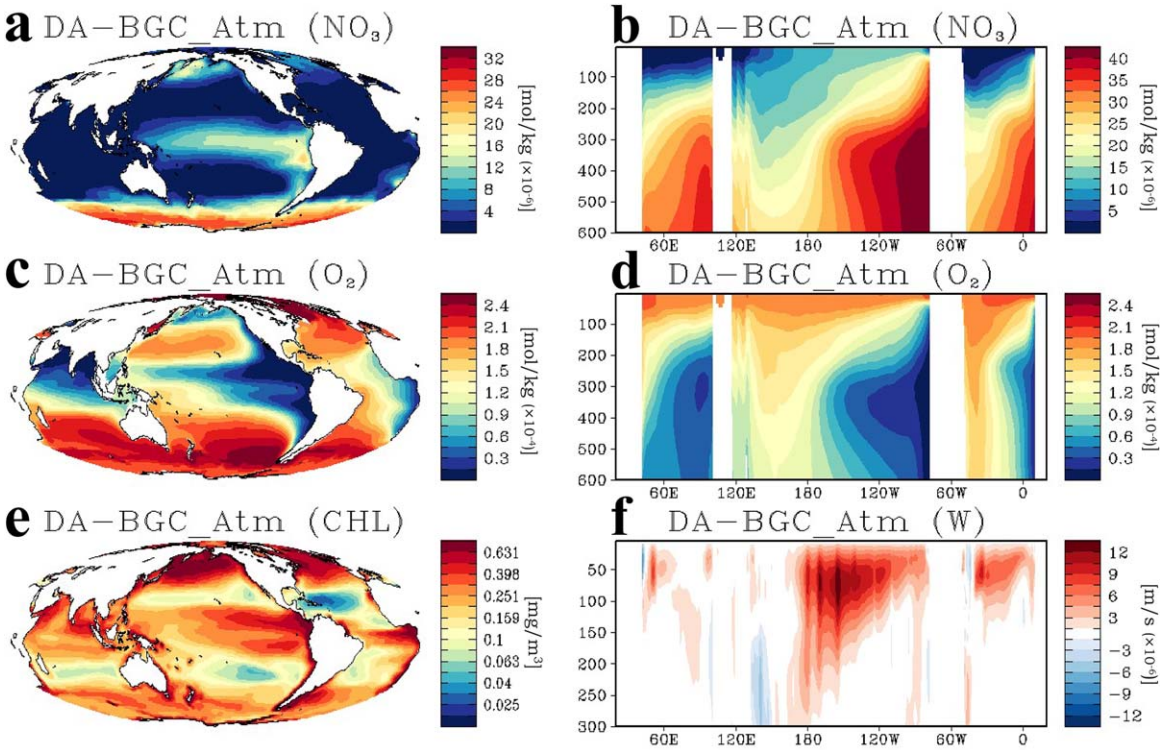


**Figure 5.** (a) Annual mean surface nitrate and (b) equatorial section (averaged between 2°S and 2°N) of nitrate simulated from the data assimilation run with a strong atmospheric data constraint (DA-BGC_Atm). (c) Subsurface oxygen averaged in 200–600 m depth, and (d) equatorial section of oxygen. Plots (e–f) are similar to (a–b) but for surface chlorophyll and equatorial section of vertical velocity, respectively.

Imposing stronger atmospheric data constraints reduces the high wind speed bias in tropical Pacific easterlies (Figure 4) and consequently reduces equatorial upwelling compared to DA-BGC (Figure 5). However, the upwelling structure in this DA-BGC_Atm run still shows large discrepancies with that in CTRL and vertical striations of potentially spurious upwelling align with equatorial TOGA-TAO mooring array measurements (Hayes et al., 1991), similar to DA-BGC (cf. Figures 5f and 2h). Moreover, the substantial biogeochemical biases present in the DA-BGC run remain. For example, the upper level nitrate and chlorophyll is still too high compared to the observations and elevated relative to the CTRL (cf. Figures 5a and 1a). The subsurface oxygen minimum in the equatorial Pacific is too weak below 200 m depth and the hypoxic center is shallower than observations. The correlation map between simulated chlorophyll from DA-BGC_Atm and satellite chlorophyll is still far from providing comparable fidelity shown in CTRL (supporting information Figure S3). Overall results here show that imposing stronger atmospheric data constraints helps to reduce the spurious upwelling problem and excessive equatorial productivity, but this is not enough to recover the fidelity without assimilation shown in CTRL.

### 4.2. The Effect of Stricter Fidelity to Ocean Model Dynamics at the Equator

Figure 6 shows the mean vertical velocity and the mean bias of nitrate at the equator simulated from the sensitivity experiments using different relative weightings of ocean data and model constraints. The observational standard errors of temperature here are inflated up to an extreme value of $10^{6}$°C from the default setting of 0.5°C (for salinity, inflated up to $2 \times 10^{5}$ g kg$^{-1}$ from 0.1 g kg$^{-1}$) and run for 5 years (2001–2005) after 1 year spin-up period (see Methods). When a weak ocean data constraint (i.e., T_obs_error = 5°C) is applied, the magnitude and striation of the equatorial vertical velocity are decreased compared to the run with the default observational standard errors (cf. Figures 6a and 6c). Moreover, the spurious upwelling column along the eastern boundary of the tropical Pacific disappears when using weak ocean data constraints. Consistent with the reduction of spurious upwelling, the excessive equatorial nitrate is also considerably reduced with the weak ocean data constraints (cf. Figures 6b and 6d). Further improvements in equatorial upwelling and nitrate simulations are observed in the experiment using higher observational standard

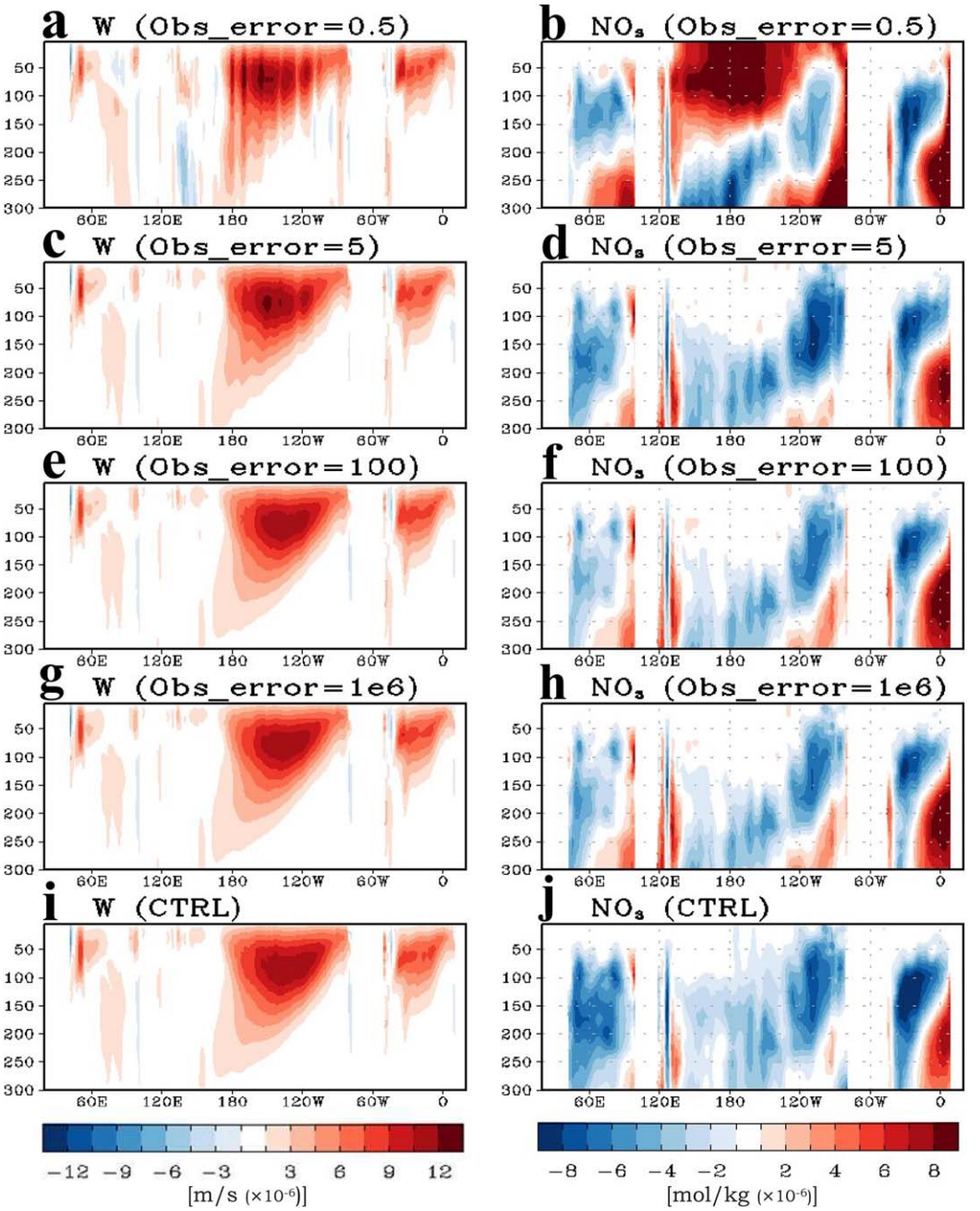


**Figure 6.** (left plot) Equatorial section of annual mean vertical velocity and (right plot) mean bias of nitrate simulated from the data assimilation runs with different observational standard errors in temperature, ranging from 0.5 to $10^{6}$°C. Higher ocean observational error refers to weaker ocean data constraint. The same rate of inflation of observational errors is also applied to salinity. The mean nitrate bias is calculated with respect to the observation.

errors (e.g., T_obs_error = 100 or $10^{6}$°C), showing less evidence of spurious equatorial upwelling and more realistic nitrate than the run with T_obs_error = 5°C.

Strengthening the model constraint relative to the data at the equator can clearly remove spurious velocities, but is there a combination that removes spurious velocities while still deriving some benefit from data assimilation? To quantify the improvement of subsurface physical and biological fields, the root-mean-square difference (RMSD) of equatorial temperature, nitrate, and oxygen from surface to 600 m depth are calculated (Figure 7). Although the weakened ocean data constraint results in a trade-off between

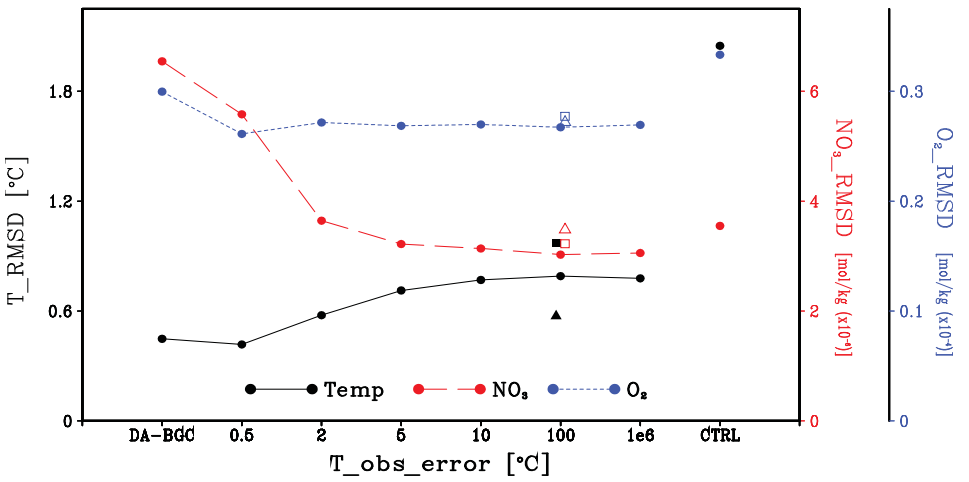


**Figure 7.** The root-mean-square difference (RMSD) of simulated subsurface equatorial (2°S–2°N; sfc-600 m) temperature (black), nitrate (red), and oxygen (blue) compared to observations (temperature from EN4 data set, and nitrate and oxygen from WOA data sets). Various observational temperature standard errors ranging from 0.5°C (default) to $10^{6}$°C are used in this sensitivity experiments using the 10°S–10°N latitudinal extent of data uncertainty inflation. Triangle and rectangle marks represent the results from two extra runs with different latitudinal extents of data uncertainty inflation, 2°S–2°N and 20°S–20°N, respectively. The RMSDs of temperature and nitrate simulated from the baseline (DA-BGC) and control (CTRL) run are also presented for the comparison with results from the sensitivity experiments.

mitigating biogeochemistry bias and increasing temperature bias, the degradation of temperature field relative to DA-BGC is not substantial. The temperature RMSDs from the different sensitivity runs are generally much lower than that from CTRL. Nitrate RMSD, in contrast, declines substantially as dynamical integrity within the model is weighted above data constraints, supporting biogeochemical gains at the equator even when data assimilation is weakened. Compared to the dramatic improvement of nitrate simulations with inflating data uncertainty, the performance of oxygen simulation is relatively stable across data assimilation variants, but all are better than the control run even with small inflations of data uncertainty. These gains are in addition to substantial improvements across other parts of the global ocean where strong oceanic data constraints are maintained (see section 5).

It is notable that the data assimilation run using extremely high data uncertainty (i.e., T_obs_error = $10^{6}$°C, equivalent to no equatorial ocean data assimilation) also shows biogeochemical gains similar to weak data assimilation runs. This is because the primary improvements at the equator in the weak assimilation runs arise from off-equatorial constraints that propagate inward via a combination of the 10° decorrelation scale and the linear ramp-up of the error inflation from 10°S/°N. This can be seen in the comparison of characteristic temperature correction increments associated with assimilation for each experiment (Figure 8). Significant increments extend below 5°N/S with both T_obs_error = 100°C and $10^{6}$°C before becoming vanishingly small in the 2° latitudinal band immediately around the equator. Improvements are thus seen at the equator despite these small increments due to the off-equatorial constraints.

To further explore the impact of off-equatorial increments, we examine the experiments using different latitudinal bands for the inflation of data uncertainty, 2°S–2°N and 20°S–20°N, keeping the observational standard error at the equator the same as in the weak assimilation (T_obs_error = 100°C). The run with the narrow latitudinal band of 2°S–2°N shows the degradation of biogeochemical simulation compared to the run with the original latitudinal ramp in 10°S–10°N band (cf. circle and triangle marks in Figure 7). Given that the 2°S–2°N run still shows strong temperature increments at and near the equator (supporting information Figure S4a), the degradation is caused by the spurious upwelling problem as seen in other strong data constraint runs such as the run with T_obs_error = 2°C. In the 20°S–20°N run, the degradation of biogeochemical simulation is reduced compared to the 2°S–2°N run, but its performance is still degraded compared to the 10°S–10°N run due to weakened off-equatorial data constraints in the 20°S–20°N run (supporting information Figure S4c). Overall, these results imply an optimal strategy of sufficiently weakening the equatorial (2°S–2°N) ocean data assimilation to suppress spurious upwelling while maximizing the positive impacts of off-equatorial increments.

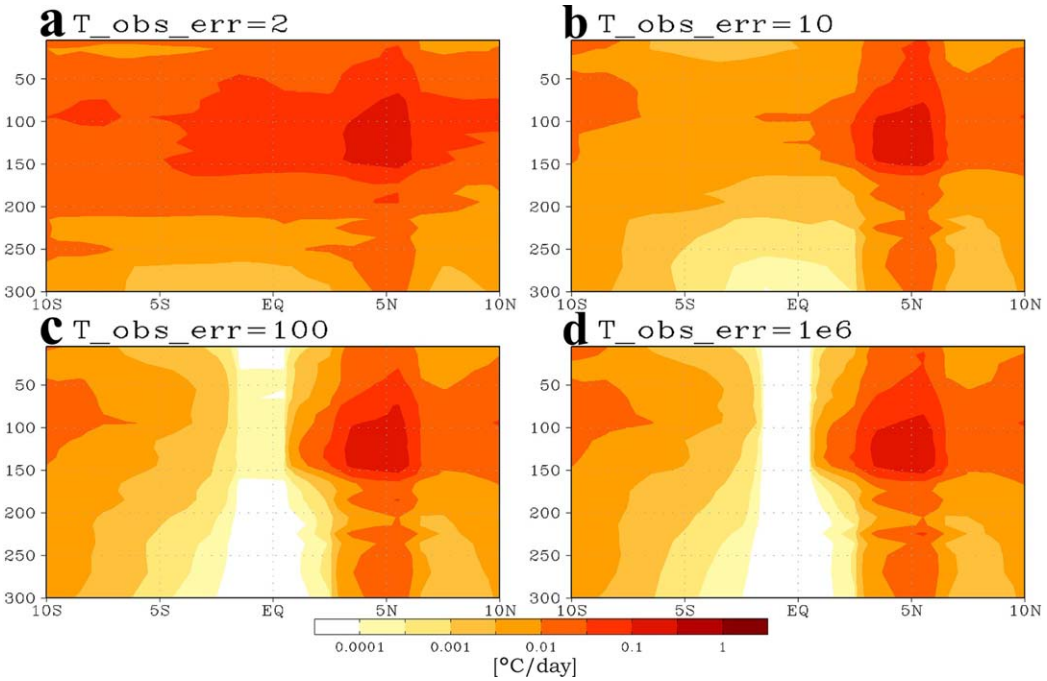


**Figure 8.** The zonally averaged standard deviation of temperature increments from sensitivity runs with various observational standard errors of (a) 2°C, (b) 10°C, (c) 100°C, and (d) $10^6$°C.

The result above supports that a weaker equatorial ocean data constraint relative to the model fidelity successfully resolves excessive equatorial production without substantially sacrificing fidelity with physical fields. Based on the finding in this section, we define our optimal run, DA-BGC_opt, as the one with strong atmosphere data constraint (Wind_obs_error = 0.1 $ms^{-1}$) and weak ocean equatorial data constraint with the latitudinal ramp in 10°S–10°N band (T_obs_error = 100°C). Although other runs with weak ocean equatorial data constraint (e.g., T_obs_error = 10°C) show the good performance in simulating mean equatorial biogeochemical fields as seen in Figure 7, we found that the observational error of 10°C is not enough to avoid degradations in temporal correlation skill of equatorial chlorophyll. Biogeochemical improvements and trade-offs reflected in this optimal run relative to CTRL and default (DA-BGC) alternatives are explored further in the next section.

## 5. Improved Biogeochemistry With Modified Assimilation Method

The mean and variability of marine biogeochemistry simulated by DA-BGC_opt shows much better agreement with the observation than that simulated by DA-BGC. The high tropical chlorophyll concentration in DA-BGC is reduced in DA-BGC_opt (Figure 9a). Variability of equatorial chlorophyll in DA-BGC_opt is also in a good agreement with observations, largely recovering the fidelity shown in CTRL (cf. Figures 9b and 3). The temporal correlation coefficients of the simulated versus observed chlorophyll in NINO3.4 region (170°W–

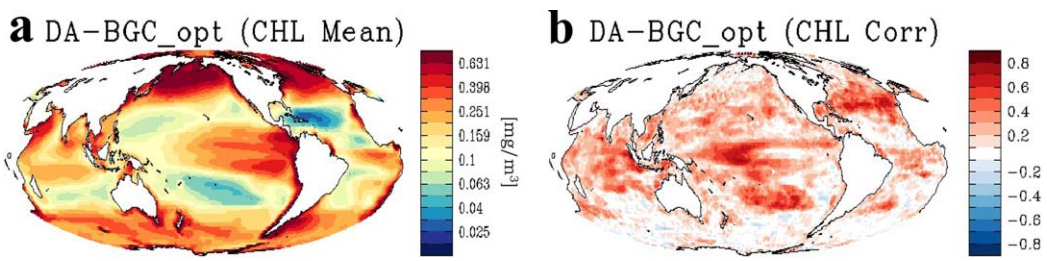


**Figure 9.** (a) Annual mean surface chlorophyll simulated from DA-BGC_opt. (b) Correlation map of chlorophyll between DA-BGC_opt and satellite data.

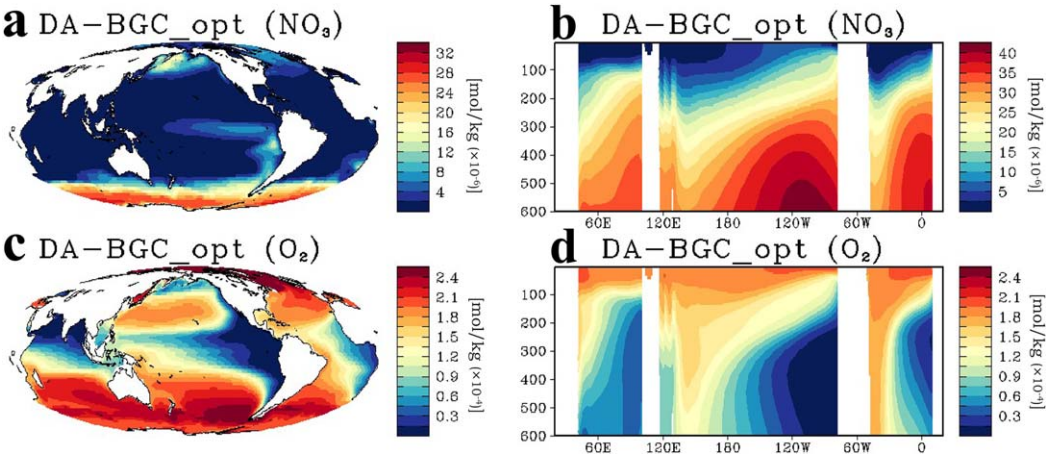


**Figure 10.** (a) The annual mean surface nitrate and (b) the equatorial section of nitrate simulated from the modified data assimilation run, DA-BGC_opt. (c) The annual mean subsurface oxygen averaged in 200–600 m depth and (d) the equatorial section of oxygen simulated from DA-BGC_opt.

120°W, 5°S–5°N) are 0.54 in DA-BGC_opt and −0.11 in DA-BGC, which is a notable improvement in the biological field compared to the relatively minor trade-off in SST correlations, 0.97 in DA-BGC_opt and 0.98 in DA-BGC in the same region. Compared to CTRL, the chlorophyll correlation skill in DA-BGC_opt is slightly worse in NINO3.4 region (0.54 in DA-BGC_opt versus 0.63 in CTRL), while improved skill is apparent in the subtropics and higher latitudes, particularly in the Atlantic (supporting information Figure S5b). The marked improvement in the chlorophyll correlation skill in DA-BGC_opt relative to CTRL is probably due to a better representation of North Atlantic mixed layer that in turn improves chlorophyll simulation in the transition zone between the warm-temperate and cold north Atlantic zones (supporting information Figure S6).

The tropical surface nitrate from DA-BGC_opt is also very similar in both pattern and magnitude to that from the observation, indicating successful reduction of excessive nutrients in the tropics shown in DA-BGC (Figure 10). Biogeochemical gains in DA-BGC_opt compared to CTRL are also notable (Figure 11). Although the DA-BGC_opt and CTRL runs simulate very similar surface nitrate fields along the equator, the subsurface nitrate from DA-BGC_opt is more consistent with the observation than that from CTRL, particularly when comparing the subsurface nitrate in the Indian Ocean and at the eastern Pacific boundary. The total RMSD and pattern correlation between observed and simulated equatorial subsurface nitrate are 2.80 $\mu$mol kg$^{-1}$ and 0.97 for DA-BGC_opt, and 3.60 $\mu$mol kg$^{-1}$ and 0.96 for CTRL, respectively.

The simulated subsurface hypoxia is also improved in the DA-BGC_opt run (Figures 10c and 10d). The underestimation of equatorial subsurface oxygen found in DA-BGC, which is presumably caused by

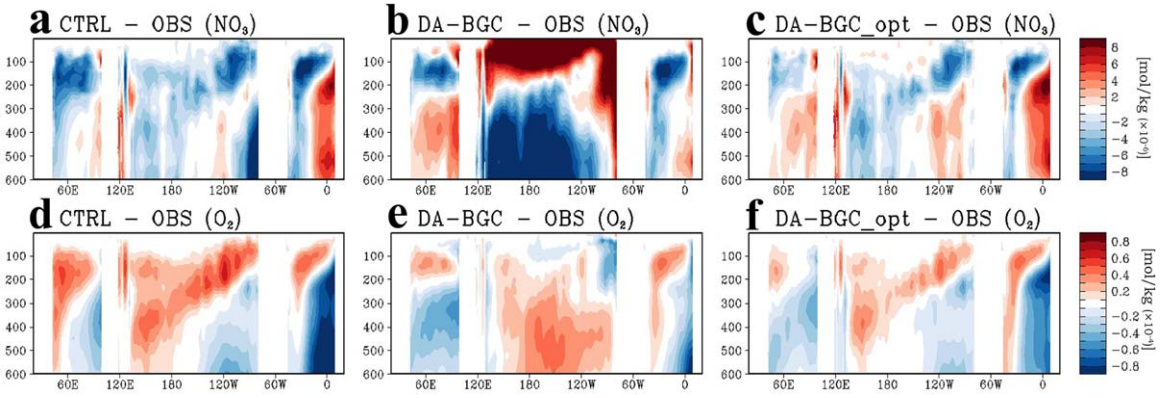


**Figure 11.** The equatorial mean nitrate difference from the observation simulated in (a) CTRL, (b) DA-BGC, and (c) DA-BGC_opt. Plots (d–f) are similar to (a–c) except for oxygen.

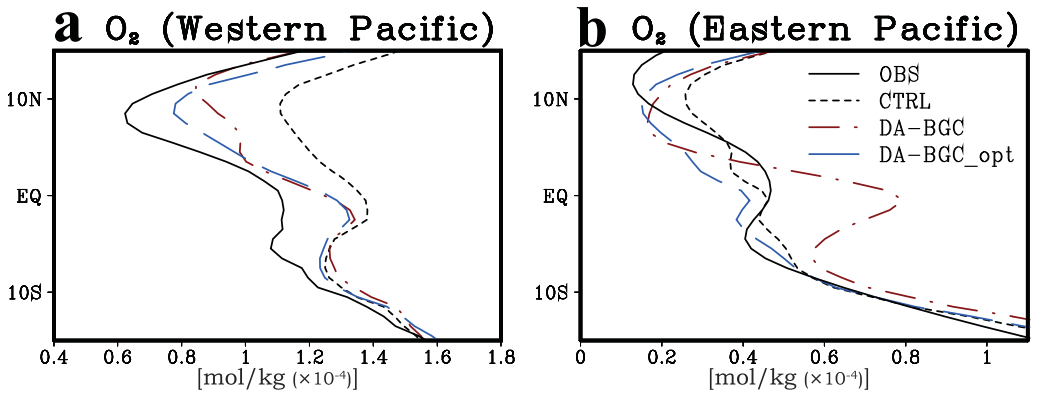


**Figure 12.** (left plot) The mean subsurface (averaged in 200–600 m depth) oxygen longitudinally averaged in the (a) western Pacific (120°E–180°E) and (b) eastern Pacific (160°W–100°W) from the observation (black), CTRL (black dashed), DA-BGC (red), and DA-BGC_opt (blue).

unphysical ventilation due to spurious vertical velocities, is no longer pronounced in DA-BGC_opt. The subsurface oxygen is still underestimated in DA-BGC_opt compared to the observation, but this bias is reduced relative to the CTRL (Figures 11d and 11f), and the vertical location of equatorial hypoxic center is better represented in DA-BGC_opt than in DA-BGC (Figures 2f and 10d). Furthermore, observed hypoxia in the north equatorial western Pacific is well captured in DA-BGC_opt, while that is absent in CTRL (Figure 12a). Similar improvement can be found in the meridional structure and magnitude of subsurface hypoxia in the eastern Pacific, particularly compared with DA-BGC (Figure 12b).

Summary statistics quantifying the performance of the simulated biogeochemistry are presented in Figure 13 (Taylor, 2001). Global mean and equatorial cross sections of nitrate, oxygen, and chlorophyll are used for computing pattern correlation, standard deviation, and centered and total RMSD. The CTRL run, in which ocean data assimilation is not applied, is generally in good agreement with observations showing pattern correlations of over 0.9 for the global patterns of nitrate and oxygen, and 0.6 for that of chlorophyll (Figure 13a). When applying baseline data assimilation methods (DA-BGC), however, the simulated nitrate and chlorophyll are degraded, lying farther from observations than CTRL, while oxygen is improved despite spurious vertical velocities at the equator. The improvement of oxygen simulation in part reflects the presence of a large low oxygen bias in the CTRL simulation. Spurious vertical velocities in DA-BGC remove this bias,

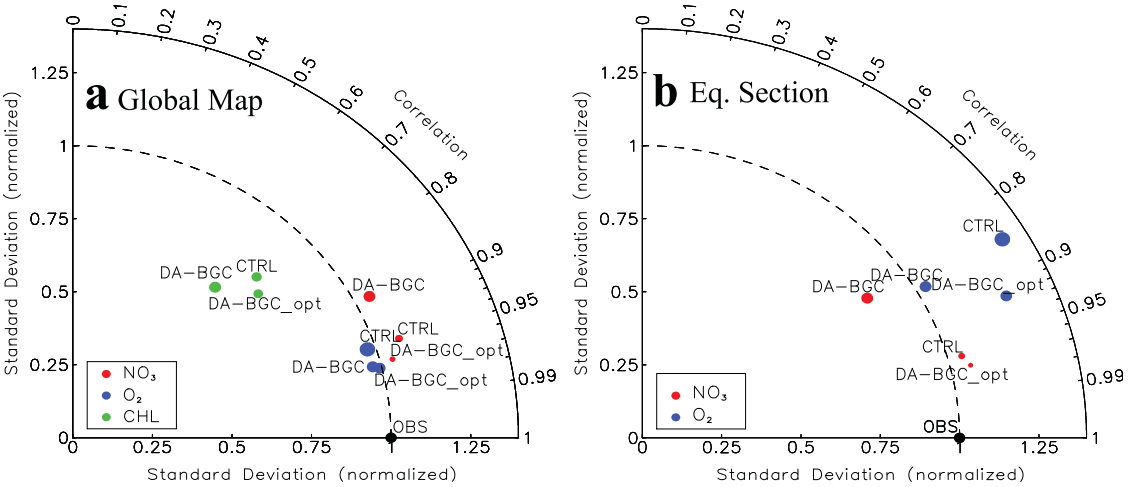


**Figure 13.** Taylor diagram for summarizing performance of different data assimilation runs. The statistics including spatial correlation, normalized standard deviation, and centered (or equivalently unbiased) root-mean-square difference (RMSD) are calculated based on the (a) global map and (b) equatorial section (2°S–2°N; sfc-600 m) of nitrate, oxygen, and chlorophyll. The statistics for equatorial section of chlorophyll is omitted due to the lack of observations. The size of each dot represents the total RMSD normalized by RMSD in DA-BGC.

though the correction overshoots the initial bias to create an over-ventilated state (Figure 2f). Similar results can be found for the equatorial section of nitrate and oxygen simulations (Figure 13b).

The DA-BGC_opt run largely resolves the issue in DA-BGC and generally shows robust agreement with chlorophyll, nitrogen and oxygen. Skill has improved for all variables relative to the control, and skill has improved markedly relative to DA-BGC for chlorophyll and nitrate. The only exception is oxygen, where DA-BGC_opt shows a marked improvement relative to the CTRL but is slightly less skillful for the bias-corrected standard deviation at the equator. The degradation of oxygen in DA-BGC_opt compared to DA-BGC is because the simulation reverts back to underestimated subsurface oxygen in the Atlantic Ocean (Figures 11e and 11f; supporting information Figure S7d), though this feature has still been greatly improved relative to CTRL. Furthermore, the skills in DA-BGC is partly rooted in artificial ocean ventilation via spurious velocities (supporting information Figure S8) that presumably compensate for other model deficiencies. Overall results indicate that physical ocean data assimilation helps to improve simulated subsurface biogeochemistry fields relative to the unconstrained run when the momentum imbalance problem at the equator is ameliorated by maintaining stronger fidelity with the dynamical model solution.

## 6. Conclusion

This study suggests a viable, pragmatic approach to integrate an ocean biogeochemical model with an ensemble coupled-climate data assimilation system. The major obstacle impeding the integration of data assimilative ocean physics and biogeochemical modeling is the inevitable dynamical imbalance errors in the assimilated system, particularly at the equator. The momentum imbalance problem enhances equatorial upwelling, leading to excessive surface nutrients and productivity. This spurious upwelling caused by data assimilation is efficiently suppressed by imposing stricter fidelity to the internal model dynamics over data constraints near the equator. Weakening the ocean data constraint resulted in a modest degradation in ocean temperature fidelity while bringing considerable biogeochemical gains. The simulated biogeochemical fields by our modified assimilation method show improved subsurface nutrient and oxygen fields at the equator compared to both the unconstrained control run and the baseline data assimilation run, except in the equatorial Atlantic. The temporal correlation skill of simulated versus observed chlorophyll in the equatorial Pacific is also improved by the modified assimilation run with respect to the baseline data assimilation run, but not exceeding the skill in the unconstrained control run. In the North Atlantic, however, the chlorophyll correlation skill in the modified assimilation run turned out to be higher than that in the control run due to a better representation of North Atlantic mixed layer depth by data assimilation. Such improvements portend refined retrospective analyses of biogeochemical dynamics and a better basis for initializing biogeochemical fields in Earth system prediction systems.

Modulating the relative weighting of model versus data at the equator was a pragmatic choice driven by the recognition that ocean biogeochemistry is extremely sensitive to dynamical imbalances in this region. Efforts to reduce such imbalances during assimilation may ameliorate the need to adopt such an approach. Even the latest approaches to address this issue, however, still produce vertical velocities that far exceed those in free-running models (Waters et al., 2017). Our approach offers a means of advancing global earth system prediction in parallel with these advances in physical data assimilation—gradually retightening equatorial data constraints as advances in assimilation allow it.

The strengths and limitations in this pragmatic approach need to be weighed against the fully coupled physical-biogeochemical data assimilation. Biogeochemical assimilation can remove substantial biogeochemical biases by assimilating chlorophyll or other biogeochemical quantities (Ford & Barciela, 2017; Gregg, 2008; While et al., 2012). Such assimilation also offers an alternative means of removing the imprint of spurious vertical velocities. It should be recognized, however, that biogeochemical assimilation in such cases may be masking effects of spurious motions that remain in the simulation. Adding biogeochemical assimilation to physical assimilation would ideally improve simulated biogeochemistry relative to patterns resulting from physical ocean properties that have been universally improved, or at least not deteriorated, relative to free-running cases. The pragmatic approach presented provides a path for achieving such a robust physical platform to support further improvement via biogeochemical simulation. It is recognized, however, that down-weighting observations at the equator in favor of model dynamics at the equator

forgoes ocean state information provided by this data. The need for this compromise can hopefully be addressed by continued data assimilation advances.

**Acknowledgments**
The authors would like to thank the anonymous reviewers for helpful and constructive comments on the manuscript. The authors also would like to thank Tom Delworth and Fernando Gonzalez-Taboada for internal reviews of the manuscript. This work was supported by NOAA's marine ecosystem tipping points initiative. The model simulation data used here are archived at GFDL (ftp://nomads.gfdl.noaa.gov/users/Jong-Yeon.Park/ECDA-COBALT/GFDL-CM2.1-COBALT/).

## References

Anderson, L. A., Robinson, A. R., & Lozano, C. J. (2000). Physical and biological modeling in the Gulf Stream region. I: Data assimilation methodology, *Deep Sea Research Part I*, *47*(10), 1787–1827.

Balmaseda, M. A., Dee, D., Vidard, A., & Anderson, D. L. T. (2007). A multivariate treatment of bias for sequential data assimilation: Application to the tropical oceans. *Quarterly Journal of the Royal Meteorological Society*, *133*(622), 167–179.

Balmaseda, M. A., Mogensen, K., & Weaver, A. T. (2013). Evaluation of the ECMWF ocean reanalysis system ORAS4. *Quarterly Journal of the Royal Meteorological Society*, *139*(674), 1132–1161.

Behringer, D. W., Ji, M., & Leetmaa, A. (1998). An improved coupled model for ENSO prediction and implications for ocean initialization. Part I: The Ocean Data Assimilation System. *Monthly Weather Review*, *126*(4), 1013–1021.

Bell, M. J., Martin, M. J., & Nichols, N. K. (2004). Assimilation of data into an ocean model with systematic errors near the equator. *Quarterly Journal of the Royal Meteorological Society*, *130*(598), 873–893.

Brasseur, P., Gruber, N., Barciela, R., Brander, K., Doron, M., El Moussaoui, A., et al. (2009). Integrating biogeochemistry and ecology into ocean data assimilation systems. *Oceanography*, *22*(3), 206–215.

Burgers, G., Balmaseda, M. A., Vossepoel, F. C., van Oldenborgh, G. J., & van Leeuwen, P. J. (2002). Balanced ocean-data assimilation near the equator. *Journal of Physical Oceanography*, *32*(9), 2509–2519.

Carton, J. A., & Giese, B. S. (2008). A reanalysis of ocean climate using Simple Ocean Data Assimilation (SODA). *Monthly Weather Review*, *136*(8), 2999–3017.

Chang, Y. S., Rosati, A., & Zhang, S. Q. (2011). A construction of pseudo salinity profiles for the global ocean: Method and evaluation. *Journal of Geophysical Research*, *116*, C02002. https://doi.org/10.1029/2010JC006386

Chang, Y. S., Zhang, S., Rosati, Q. A., Delworth, T. L., & Stern, W. F. (2013). An assessment of oceanic variability for 1960–2010 from the GFDL ensemble coupled data assimilation. *Climate Dynamics*, *40*(3–4), 775–803.

Chust, G., Allen, J. I., Bopp, L., Schrum, C., Holt, J., Tsiaras, K., et al. (2014). Biomass changes and trophic amplification of plankton in a warmer ocean. *Global Change Biology*, *20*(7), 2124–2139.

Ciavatta, S., Torres, R., Martinez-Vicente, V., Smyth, T., Dall'Olmo, G., Polimene, L., et al. (2014). Assimilation of remotely-sensed optical properties to improve marine biogeochemistry modelling. *Progress in Oceanography*, *127*, 74–95.

Danabasoglu, G., Yeager, S. G., Bailey, D., Behrens, E., Bentsen, M., Bi, D., et al. (2014). North Atlantic simulations in Coordinated Ocean-ice Reference Experiments phase II (CORE-II). Part I: Mean states. *Ocean Modelling*, *73*, 76–107.

Delworth, T. L., Broccoli, A. J., Rosati, A., Stouffer, R. J., Balaji, V., Beesley, J. A., et al. (2006). GFDL's CM2 global coupled climate models. Part I: Formulation and simulation characteristics. *Journal of Climate*, *19*(5), 643–674.

Edwards, C. A., Moore, A. M., Hoteit, I., & Cornuelle, B. D. (2015). Regional ocean data assimilation. *Annual Review of Marine Science*, *7*, 21–42.

Esaias, W. E., Abbott, M. R., Barton, I., Brown, O. B., Campbell, J. W., Carder, K. L., et al. (1998). An overview of MODIS capabilities for ocean science observations. *IEEE Transactions on Geoscience and Remote Sensing*, *36*(4), 1250–1265.

Fontana, C., Grenz, C., Pinazo, C., Marsaleix, P., & Diaz, F. (2009). Assimilation of SeaWiFS chlorophyll data into a 3D-coupled physical-biogeochemical model applied to a freshwater-influenced coastal zone. *Continental Shelf Research*, *29*(11–12), 1397–1409.

Ford, D. A., & Barciela, R. M. (2017). Global marine biogeochemical reanalyses assimilating two different sets of merged ocean colour products. *Remote Sensing of Environment*, *203*, 40–54.

Ford, D. A., & Barciela, R. M. (2015). *Marine biogeochemical data assimilation—Literature review and scoping report* (Rep. 609, pp. 21–25). Exeter, UK: Met Office.

Ford, D. A., Edwards, K. P., Lea, D., Barciela, R. M., Martin, M. J., & Demaria, J. (2012). Assimilating GlobColour ocean colour data into a pre-operational physical-biogeochemical model. *Ocean Science*, *8*(5), 751–771.

Garcia, H. E., Locarnini, R. A., Boyer, T. P., Antonov, J. I., Baranova, O. K., Zweng, M. M., et al. (2010a). *World ocean atlas 2009, vol. 3: Dissolved oxygen, apparent oxygen utilization, and oxygen saturation* (NOAA Atlas NESDIS 70). Washington, DC: U.S. Government Printing Office.

Garcia, H. E., Locarnini, R. A., Boyer, T. P., Antonov, J. I., Zweng, M. M., Baranova, O. K., et al. (2010b). *World ocean atlas 2009, vol. 4: Nutrients (phosphate, nitrate, silicate)* (NOAA Atlas NESDIS 71). Washington, DC: U.S. Government Printing Office.

Good, S. A., Martin, M. J., & Rayner, N. A. (2013). EN4: Quality controlled ocean temperature and salinity profiles and monthly objective analyses with uncertainty estimates. *Journal of Geophysical Research*, *118*(12), 6704–6716.

Gregg, W. W. (2008). Assimilation of SeaWiFS ocean chlorophyll data into a three-dimensional global ocean model. *Journal of Marine Systems*, *69*(3–4), 205–225.

Gregg, W. W., Rousseaux, C. S., & Franz, B. A. (2017). Global trends in ocean phytoplankton: A new assessment using revised ocean colour data. *Remote Sensing Letters*, *8*(12), 1102–1111.

Griffies, S. M., Biastoch, A., Böning, C., Bryan, F., Danabasoglu, G., Chassignet, E. P., et al. (2009). Coordinated Ocean-ice Reference Experiments (COREs). *Ocean Modelling*, *26*(1–2), 1–46.

Griffies, S. M., Yin, J., Durack, P. J., Goddard, P., Bates, S. C., Behrense, E., et al. (2014). An assessment of global and regional sea level for years 1993–2007 in a suite of interannual CORE-II simulations. *Ocean Modelling*, *78*, 35–89.

Hawkins, E., & Sutton, R. (2009). The potential to narrow uncertainty in regional climate predictions. *Bulletin of the American Meteorological Society*, *90*(8), 1095–1107.

Hayes, S. P., Mangum, L. J., Picaut, J., Sumi, A., & Takeuchi, K. (1991). TOGA-TAO: A moored array for real-time measurements in the Tropical Pacific Ocean. *Bulletin of the American Meteorological Society*, *72*(3), 339–347.

Hemmings, J. C. P., Barciela, R. M., & Bell, M. J. (2008). Ocean color data assimilation with material conservation for improving model estimates of air-sea CO(2) flux. *Journal of Marine Research*, *66*(1), 87–126.

Henson, S. A., Sarmiento, J. L., Dunne, J. P., Bopp, L., Lima, I., Doney, S. C., et al. (2010). Detection of anthropogenic climate change in satellite records of ocean chlorophyll and productivity. *Biogeosciences*, *7*(2), 621–640.

Hoteit, I., Cornuelle, B., & Heimbach, P. (2010). An eddy-permitting, dynamically consistent adjoint-based assimilation system for the tropical Pacific: Hindcast experiments in 2000. *Journal of Geophysical Research*, *115*, C03001. https://doi.org/10.1029/2009JC005437

Ishizaka, J. (1990). Coupling of coastal zone color scanner data to a physical-biological model of the Southeastern U.S. Continental Shelf Ecosystem: 3. Nutrient and phytoplankton fluxes and CZCS data assimilation. *Journal of Geophysical Research*, *95*(C11), 20201–20212.

Kanamitsu, M., Ebisuzaki, W., Woollen, J., Yang, S. K., Hnilo, J. J., Fiorino, M., et al. (2002). NCEP-DOE AMIP-II reanalysis (R-2). *Bulletin of the American Meteorological Society*, *83*(11), 1631–1643.
Kearney, K. A., Stock, C., & Sarmiento, J. L. (2013). Amplification and attenuation of increased primary production in a marine food web. *Marine Ecology Progress Series*, *491*, 1–14.
Key, R. M., Kozyr, A., Sabine, C., Lee, L., Wanninkhof, K. R., Bullister, J. L., et al. (2004). A global ocean carbon climatology: Results from Global Data Analysis Project (GLODAP). *Global Biogeochemical Cycles*, *18*, GB4031. https://doi.org/10.1029/2004GB002247
Kohl, A., & Stammer, D. (2008). Variability of the meridional overturning in the North Atlantic from the 50-year GECCO state estimation. *Journal of Physical Oceanography*, *38*(9), 1913–1930.
Large, W. G., & Yeager, S. G. (2009). The global climatology of an interannually varying air-sea flux data set. *Climate Dynamics*, *33*(2–3), 341–364.
Lee, K. W., Yeh, S. W., Kug, J. S., & Park, J. Y. (2014). Ocean chlorophyll response to two types of El Nino events in an ocean-biogeochemical coupled model. *Journal of Geophysical Research*, *119*, 933–952. https://doi.org/10.1002/2013JC009050
McClain, C. R., Cleave, M. L., Feldman, G. C., Gregg, W. W., Hooker, S. B., & Kuring, N. (1998). Science quality SeaWiFS data for global biosphere research. *Sea Technology*, *39*(9), 10–16.
Mollmann, C., Folke, Edwards, C. M., & Conversi, A. (2015). Marine regime shifts around the globe: Theory, drivers and impacts. *Philosophical Transactions of the Royal Society B*, *370*(1659), 20130260.
Myers, R. A. (1998). When do environment-recruitment correlations work? *Reviews in Fish Biology and Fisheries*, *8*(3), 285–305.
Natvik, L. J., & Evensen, G. (2003). Assimilation of ocean colour data into a biochemical model of the North Atlantic—Part 1. Data assimilation experiments. *Journal of Marine Systems*, *40*, 127–153.
Pelc, J. S., Simon, E., Bertino, L., El Serafy, G., & Heemink, A. W. (2012). Application of model reduced 4D-Var to a 1D ecosystem model. *Ocean Modelling*, *57–58*, 43–58.
Raghukumar, K., Edwards, C. A., Goebel, N. L., Broquet, G., Veneziani, M., Moore, A. M., et al. (2015). Impact of assimilating physical oceanographic data on modeled ecosystem dynamics in the California Current System. *Progress in Oceanography*, *138*, 546–558.
Reynolds, R. W., Smith, T. M., Liu, C., Chelton, D. B., Casey, K. S., & Schlax, M. G. (2007). Daily high-resolution-blended analyses for sea surface temperature. *Journal of Climate*, *20*(22), 5473–5496.
Saha, S., Moorthi, S., Wu, X., Wang, J., Nadiga, S., Tripp, P., et al. (2014). The NCEP Climate Forecast System Version 2. *Journal of Climate*, *27*(6), 2185–2208.
Shulman, I., Frolov, S., Anderson, S., Penta, B., Gould, R., Sakalaukus, P., et al. (2013). Impact of bio-optical data assimilation on short-term coupled physical, bio-optical model predictions. *Journal of Geophysical Research*, *118*, 2215–2230. https://doi/org/10.1002/jgrc.20177
Song, H., Edwards, C. A., Moore, A. M., & Fiechter, J. (2016). Data assimilation in a coupled physical-biogeochemical model of the California Current System using an incremental lognormal 4-dimensional variational approach: Part 1—Model formulation and biological data assimilation twin experiments. *Ocean Modelling*, *106*, 131–145.
Stock, C. A., Dunne, J. P., & John, J. G. (2014a). Drivers of trophic amplification of ocean productivity trends in a changing climate. *Biogeosciences*, *11*(24), 7125–7135.
Stock, C. A., Dunne, J. P., & John, J. G. (2014b). Global-scale carbon and energy flows through the marine planktonic food web: An analysis with a coupled physical-biological model. *Progress in Oceanography*, *120*, 1–28.
Stock, C. A., John, J. G., Rykaczewski, R. R., Asch, R. G., Cheung, W. W. L., Dunne, J. P., et al. (2017). Reconciling fisheries catch and ocean productivity. *Proceedings of the National Academy of Sciences of the United States of America*, *114*(8), E1441–E1449.
Storto, A., Masina, S., & Navarra, A. (2016). Evaluation of the CMCC eddy-permitting global ocean physical reanalysis system (C-GLORS, 1982–2012) and its assimilation components. *Quarterly Journal of the Royal Meteorological Society*, *142*(695), 738–758.
Tagliabue, A., Aumont, O., DeAth, R., Dunne, J. P., Dutkiewicz, S., Galbraith, E., et al. (2016). How well do global ocean biogeochemistry models simulate dissolved iron distributions? *Global Biogeochemical Cycles*, *30*(2), 149–174.
Taylor, K. E. (2001). Summarizing multiple aspects of model performance in a single diagram. *Journal of Geophysical Research*, *106*(D7), 7183–7192.
Tommasi, D., Stock, C. A., Hobday, A. J., Methot, R., Kaplan, I. C., Eveson, J. P., et al. (2017a). Managing living marine resources in a dynamic environment: The role of seasonal to decadal climate forecasts. *Progress in Oceanography*, *152*, 15–49.
Tommasi, D., Stock, C. A., Pegion, K., Vecchi, G. A., Methot, R. D., Alexander, M. A., et al. (2017b). Improved management of small pelagic fisheries through seasonal climate prediction. *Ecological Applications*, *27*(2), 378–388.
Valsala, V., & Maksyutov, S. (2010). Simulation and assimilation of global ocean pCO(2) and air-sea $CO_2$ fluxes using ship observations of surface ocean pCO(2) in a simplified biogeochemical offline model. *Tellus Series B*, *62*(5), 821–840.
Vidard, A., Anderson, D. L. T., & Balmaseda, M. (2007). Impact of ocean observation systems on ocean analysis and seasonal forecasts. *Monthly Weather Review*, *135*(2), 409–429.
Waters, J., Bell, M. J., Martin, M. J., & Lea, D. J. (2017). Reducing ocean model imbalances in the equatorial region caused by data assimilation. *Quarterly Journal of the Royal Meteorological Society*, *143*(702), 195–208.
Watson, J. R., Stock, C. A., & Sarmiento, J. L. (2015). Exploring the role of movement in determining the global distribution of marine biomass using a coupled hydrodynamic—Size-based ecosystem model. *Progress in Oceanography*, *138*, 521–532.
While, J., Haines, K., & Smith, G. (2010). A nutrient increment method for reducing bias in global biogeochemical models. *Journal of Geophysical Research*, *115*, C10036. https://doi.org/10.1029/2010JC006142
While, J., Totterdell, I., & Martin, M. (2012). Assimilation of pCO(2) data into a global coupled physical-biogeochemical ocean model. *Journal of Geophysical Research*, *117*, C03037. https://doi.org/10.1029/2010JC006815
Yang, X. S., Rosati, A., Zhang, S., Delworth, T. L., Gudgel, R. G., Zhang, R., et al. (2013). A predictable AMO-like pattern in the GFDL fully coupled ensemble initialization and decadal forecasting system. *Journal of Climate*, *26*(2), 650–661.
Zhang, S., Harrison, M. J., Rosati, A., & Wittenberg, A. (2007). System design and evaluation of coupled ensemble data assimilation for global oceanic climate studies. *Monthly Weather Review*, *135*(10), 3541–3564.